Edinburgh Research Explorer

Staggered Coprime Pulse Repetition Frequencies Synthetic Aperture Radar (SCopSAR)

Staggered Coprime Pulse Repetition Frequencies Synthetic Aperture Radar (SCopSAR)

Abdulmalik Aldharrab, *Member, IEEE,* and Mike E. Davies, *Fellow, IEEE*

Abstract—High-Resolution Wide-Swath Synthetic Aperture Radar (HRWS-SAR) imaging is highly desirable since it allows one to produce high-resolution SAR images of large areas during a short visit time. In this paper, Staggered Coprime Pulse Repetition Frequencies Synthetic Aperture Radar (SCopSAR) is proposed. It divides the time during which a scatterer is illuminated by the antenna beam-pattern into two halves where, in each half, pulses are transmitted at the rate of one of two sub-Nyquist Pulse Repetition Frequencies (PRFs). Such PRFs are related to the Nyquist PRF using two coprime sub-sampling factors. This allows extending the maximum range swath width that can be imaged by a number of times that equals the smaller sub-sampling factor at the expense of a reduction in the azimuth resolution by half. It further allows for a reduction in the amount of data to be stored and communicated. SCopSAR is an imaging modality suitable for scenes that contain a small number of bright scatterers over a dark background which, for instance, is the case when imaging ships in a calm sea background. Compared to the techniques recently proposed in the literature, SCopSAR simplifies the Radar requirements since it uses only one carrier frequency, one waveform, and one channel. Simulations and real ERS-2 satellite raw data are used to validate the theoretical findings presented in this paper.

Index Terms—Synthetic Aperture Radar (SAR), High-Resolution Wide-Swath (HRWS), coprime sampling, sub-Nyquist, staggered PRFs, Low Pulse Repetition Frequency (LPRF), bright scatterers, ship detection.

I. INTRODUCTION

WIDE SWATH Synthetic Aperture Radar (SAR) imaging requires using a Low Pulse Repetition Frequency (LPRF) to allow reflections from the nearest and farthest points in the range swath to arrive within the listening time of one Pulse Repetition Interval (PRI). However, such an LPRF will limit the maximum Doppler bandwidth that can be unambiguously sampled which, consequently, limits the maximum azimuth resolution that can be achieved without allowing for azimuth aliasing [1]. In practice, the antenna beam-pattern is used as an anti-aliasing filter to illuminate only the region of interest in the ground and limit the level of range and azimuth aliasing in the received signal [2]–[4]. In its basic implementation, spotlight SAR continuously steers the antenna beam to focus on a specific area on the ground, as a result, the Doppler bandwidth generated due to each scatterer within such an area of interest will increase which provides an improved azimuth resolution. However, operating in spotlight mode limits the azimuth extent and the range swath that can be

Abdulmalik Aldharrab and Mike E. Davies are with the School of Engineering, Institute for Digital Communications (IDCOM), The University of Edinburgh, Edinburgh EH9 3JL, UK. (*Corresponding author: Abdulmalik Aldharrab,* e-mail: a.aldharrab@ed.ac.uk).

Abdulmalik Aldharrab is also with King Abdulaziz City for Science and Technology (KACST), Riyadh 12354, Saudi Arabia.

imaged [5]. On the other hand, a typical ScanSAR repeatedly visits multiple sub-swaths by steering the antenna beam in elevation while the platform that carries the Radar is traveling along the flight track. This allows trading azimuth resolution for an extension in the range swath [6]. De Zan and Monti Guarnieri [7] introduced Terrain Observation by Progressive Scans SAR (TOPSAR) which sweeps the antenna beam in an anti-spotlight mode in the azimuth direction while scanning each of the sub-swaths to reduce the effect of the non-ideal antenna pattern on ScanSAR. However, TOPSAR still suffers from the same resolution degradation problem of ScanSAR which is the result of a reduced dwell time on target. To improve the azimuth resolution in ScanSAR and TOPSAR, multiple along-track receive phase centers can be used [8]. An early review of the techniques that allow simultaneous High-Resolution Wide-Swath (HRWS) SAR imaging such as the use of multiple transmit or receive azimuth or elevation antenna beams is provided by Currie and Brown [9]. Recently, Krieger *et al.* [10] suggested a multi-beam technique that utilizes multiple sub-pulses or waveforms along with multiple azimuth and elevation sub-arrays or antennas to allow exploiting more of the overall antenna area to obtain high gain both on transmit and on receive. As it is the case in ScanSAR, multi-beam techniques suffer from the artifacts introduced due to the non-ideal beam-patterns which complicate the processing of the received signals. This can be overcome by using a multichannel SAR with multiple along-track displaced phase centers to allow sampling the full Doppler bandwidth while using a PRF that is smaller than the Nyquist PRF by a number of times that equals the number of receive phase centers [11]–[13].

If the scene to be imaged contains a small number of bright scatterers over a dark background which is, for instance, the case when imaging ships in a calm sea background, it is possible to achieve HRWS imaging without the need for multichannels or multi-beams. This can be achieved by sampling the synthetic aperture using properly chosen sub-Nyquist PRFs. Di Martino and Iodice recently proposed Co-prime Synthetic Aperture Radar (CopSAR) [14] and Ortogonal Coprime Synthetic Aperture Radar (OrthoCopSAR) [15] which sample the synthetic aperture using two interlaced sub-Nyquist PRFs. Dual-frequency CopSAR [14] uses one of two carrier frequencies and OrthoCopSAR [15] uses an up or a down chirp to transmit the pulses that correspond to each PRF. The use of an additional carrier frequency or waveform allows extending the maximum range swath width that can be imaged by a number of times that equals the smaller sub-sampling factor without introducing any degradation to the azimuth resolution.

In this paper, we propose SCopSAR which is an imaging modality that requires only a single waveform such as the conventional Linear Frequency-Modulated (LFM) chirp, a single carrier frequency, and a single channel. SCopSAR divides the time during which a scatterer is illuminated by the antenna beam into two halves where, in each half, one of two sub-Nyquist PRFs is used. Each of the PRFs is related to the Nyquist PRF using one of two coprime sub-sampling factors. This allows trading half the azimuth resolution for an extension in the range swath width by a number of times that equals the smaller sub-sampling factor. Using SCopSAR in spotlight mode further allows extending the maximum azimuth extent that can be covered. Moreover, SCopSAR provides a reduction in the amount of data to be stored and communicated. Compared to current HRWS imaging techniques, SCopSAR simplifies the system requirements greatly. It has been demonstrated in the literature that the use of up and down chirps introduces performance degradation for the case of spatially extended targets [16], [17], SCopSAR avoids this by using only one waveform. It is worth mentioning that the use of multiple staggered PRFs is a well-established technique that is used in pulsed Doppler Radars to resolve Doppler and range ambiguities which allows the Radar to simultaneously and unambiguously cover a long range and estimate the correct radial velocity of fast targets [18], [19]. Therefore, it is worth emphasizing that the focus of this paper is on utilizing such a sampling technique for SAR imaging.

II. STAGGERED COPRIME PRFs SAR

Consider the imaging geometry where the unit used for all the axes (x_r, u, z) is the meter. To distinguish the Radar domain from the target domain and for notational convenience, an additional axis that is denoted as the $y - axis$ and aligned to the $u - axis$ is defined for the target area [3]. The reference point of the antenna phase center is at $(x_r, u, z) = (0, 0, 0)$ and the scene center is at $(x_r, y, z) = (X_{rc}, 0, Z_c)$ where X_{rc} and Z_c are the range to the center of the target area and the antenna phase center's altitude, respectively. The platform that carries the Radar is assumed to be traveling in a straight path along the $u - axis$ which is the cross-range or azimuth domain. Therefore, (x_r, z) will be augmented into the down-range or slant-range domain $x = \sqrt{x_r^2 + z^2}$ [4]. Consequently, the down-range to the scene center is defined as $X_c = \sqrt{X_{rc}^2 + Z_c^2}$. The following LFM chirp is transmitted towards the scene of interest every $1/PRF = PRI = \Delta_u/v_p$ where Δ_u is the distance between the pulses' transmission locations in meters and v_p is the platform's velocity which is assumed uniform and independent of the down-range:

$$p(t) = \text{rect}\left(\frac{t}{T}\right)e^{j2\pi(f_c t + \beta t^2)}, \tag{1}$$

where t is the fast-time or range-time variable in seconds, T is the chirp duration, f_c is the carrier frequency, $\text{rect}(t/T) = 1$ for $|t| \leq T/2$ and zero otherwise. Moreover, the chirp rate is defined here as $\beta = BW_p/2T$ where BW_p is the chirp bandwidth.

The focus will be on a single scatterer located at (x, y). Under the narrow band assumption, after coherent down-conversion, the received signal due to such a scatterer which is assumed to be in the far field is given as:

$$s(t, u) = \sigma p(t - R(u)/c)e^{-j2\pi f_c t}, \tag{2}$$

where $R(u) = 2\sqrt{x^2 + (y - u)^2}$ is the round-trip distance to the scatterer, c is the speed of light, and σ is used to account for the reflectivity of the scatterer and the path loss. The azimuth Fourier transformed version of (2) is given as [20]:

$$S(t, k_u) = \sigma \, \text{rect}\left([t - 2x'(k_u)/c]\beta'(k_u)/\beta T\right)$$
$$e^{-j[k_u y + \sqrt{4k_c^2 - k_u^2}x]}e^{j2\pi\beta'(k_u)[t - 2x'(k_u)/c]^2}, \tag{3}$$

where k_u is the azimuth spatial frequency which will also be referred to as the Doppler frequency, $k_c = 2\pi/\lambda_c$ is the wavenumber at the carrier frequency, $\lambda_c = c/f_c$ is the wavelength at the carrier frequency, $x'(k_u) = x/\sqrt{1 - k_u^2/4k_c^2} = x[1 + C(k_u)]$, and

$$\beta'(k_u) = \beta\left[1 - \frac{2\pi\beta k_u^2 x}{k_c^3 c^2[1 - k_u^2/4k_c^2]^{3/2}}\right]^{-1}. \tag{4}$$

A. Resolution & Coverage

In general, the antenna beam-pattern provides a natural anti-aliasing filter. It limits the footprint of the Radar in the range and azimuth directions which, consequently, limits the azimuth bandwidth. A broadside target area centered at $(X_c, 0)$ and a synthetic aperture that extends from $(0, -L)$ to $(0, L)$ are considered to quantify the trade-offs in a side-looking staring spotlight SAR system. The azimuth resolution of a scatterer located at $(x, 0)$ is given as [3]:

$$\delta_u(x) = \frac{\lambda_c}{4L}x. \tag{5}$$

The minimum down-range observable to the Radar will be denoted by x_{min}. Moreover, the minimum and maximum Radar wavelengths will be defined, respectively, as λ_{min} and λ_{max}. If a planar antenna whose width in the azimuth domain is denoted by D_u is used, the Doppler bandwidth, in Hz, will be given as [3]:

$$BW_D = \frac{4v_p}{\lambda_{min}}\sin\left(\tan^{-1}\left[\frac{L + \lambda_{max} \cdot x_{min}/D_u}{x_{min}}\right]\right). \tag{6}$$

In staring spotlight SAR, the antenna beam-pattern is steered to always illuminate the same area on the ground. Consequently, the instantaneous Doppler bandwidth will be limited to $BW_D^{inst} \approx 4v_p/D_u$. Therefore, to satisfy the azimuth Nyquist sampling criterion, the separation between the pulse transmission locations should fulfill $\Delta_u \leq D_u/2$. In fact, a more conservative system will use a $\Delta_u \leq D_u/4$ to further limit the amount of azimuth aliasing in the received signal which improves the quality of the produced SAR image as detailed in [3].

In stripmap SAR, the antenna look angle is fixed during imaging, consequently, the Doppler bandwidth is a function of the Antenna Azimuth Pattern (AAP). Therefore, for a boresight acquisition geometry, the azimuth Nyquist sampling criterion is $\Delta_u \leq D_u/2$ and a more conservative system will use a $\Delta_u \leq D_u/4$ [3]. The footprint of the AAP dictates

the time duration during which a scatterer is illuminated by the antenna beam-pattern while the platform is traveling along the flight path. This is commonly referred to as the integration time and it is given at the scene center as [4]:

$$T_{int} = \frac{\lambda_c}{D_u v_p} X_c. \tag{7}$$

In stripmap mode, observing a target over its full integration time allows obtaining an azimuth resolution of $\delta_u \approx D_u/2$ [3], [4]. Let $r_{min}(u)$ and $r_{max}(u)$, respectively, denote the radial distances to the nearest and farthest scatterers in the observed scene while the Radar is at azimuth location u. To avoid introducing range aliasing, the PRF used should be chosen low enough to ensure that, at any point along the synthetic aperture:

$$\frac{1}{PRF} - 2T > 2\Delta_r(u)/c, \tag{8}$$

where $\Delta_r(u) = r_{max}(u) - r_{min}(u)$.

B. Sub-Nyquist SAR

According to the condition of (8), wide-swath SAR imaging requires using a low PRF. However, such a low PRF will limit the maximum Doppler bandwidth that can be unambiguously sampled which, consequently, limits the azimuth resolution. A low PRF will further limit the extent of the azimuth area covered in spotlight mode. Therefore, we propose SCopSAR which uses sub-Nyquist PRFs to extend the maximum range swath width that can be covered. This will introduce azimuth aliasing, however, as will be explained in Section II-C, the sub-Nyquist PRFs are chosen carefully to allow for alias removal. Another factor that motivates the need for sub-Nyquist PRFs is that the azimuth Nyquist sampling criteria are derived based on the assumption that the antenna pattern is ideal [3], [4]. However, in practice, antenna patterns are non-ideal and allow for some azimuth aliasing. Such aliasing can be reduced by using a higher PRF. However, the higher the PRF used the smaller the maximum range swath width that can be covered.

The conventional Chirp Scaling Algorithm (CSA) [21] is used here to focus each sub-Nyquist image. CSA is designed to correctly focus the SAR image under the assumption that the synthetic aperture is sampled at a Nyquist rate [21]. However, the synthetic aperture in SCopSAR is sampled at a sub-Nyquist rate. Therefore, this section provides analysis of the impact of the different CSA processing steps on the sub-Nyquist signal. Since pulses are transmitted at discrete azimuth locations, an azimuth discretized version of (3) is given as [22]:

$$Q(t, k_u) = \frac{1}{\Delta_u} \sum_l S(t, k_u - l/\Delta) = \sum_l S^l(t, k_u), \tag{9}$$

where $\Delta = \Delta_u/2\pi$. Except for the constant $1/\Delta_u$, (3) can be obtained from (9) by setting l to zero. Moreover, the CSA is derived based on the assumption that the synthetic aperture is sampled at higher than the Nyquist rate [21]. Therefore, it can be said that different processing steps in CSA are designed based on the $(l = 0)$ component of (9) which is associated with the true scatterers which will appear in the image at the correct locations and properly focused. However, due to the

mismatch between different CSA processing steps and $(l \neq 0)$ components which are associated with the aliases, aliases will appear shifted and defocused in both the azimuth and the down-range domain. The chirp scaled version of the lth component of (9) is given as [21]:

$$S_{cs}^l(t, k_u) = S^l(t, k_u)e^{j2\pi\beta'_{ref}(k_u)C(k_u)[t-2x'_{ref}(k_u)/c]^2}, \tag{10}$$

where $x'_{ref}(k_u) = x_{ref}[1 + C(k_u)]$, $\beta'_{ref}(k_u)$ is given by (4) when $x = x_{ref}$, and x_{ref} is the down-range to the reference point which can be arbitrarily chosen. Range Cell Migration Correction (RCMC) and range compression are performed by the following phase multiply in the frequency domain [21]:

$$S_{rc}^l(w, k_u) = S_{cs}^l(w, k_u) \\ e^{jw^2/8\pi\beta'_{ref}(k_u)[1+C(k_u)]}e^{j2x_{ref}C(k_u)w/c}. \tag{11}$$

The phase of (11) is given as:

$$\angle S_{rc}^l(w, k_u) = -\frac{\beta'_\Delta(k_u; l)}{8\pi\beta'_{ref}(k_u)[1 + C(k_u)]}w^2 \\ - \frac{2\beta'(k_u - l/\Delta)x'(k_u - l/\Delta)}{c[\beta'(k_u - l/\Delta) + \beta'_{ref}(k_u)C(k_u)]}w \\ - 2x_{ref}\beta'_\Delta(k_u; l)C(k_u)w/c - (k_u - l/\Delta)y \\ - \sqrt{4k_c^2 - (k_u - l/\Delta)^2}x + \Theta_\Delta(x, k_u; l), \tag{12}$$

where

$$\beta'_\Delta(k_u; l) = \frac{\beta'_{ref}(k_u) - \beta'(k_u - l/\Delta)}{\beta'_{ref}(k_u)C(k_u) + \beta'(k_u - l/\Delta)}, \tag{13}$$

and w is used to denote the fast-time temporal frequency which will also be referred to as the range-time frequency. Moreover,

$$\Theta_\Delta(x, k_u; l) = \\ \frac{8\pi\beta'(k_u - l/\Delta)\beta'_{ref}(k_u)C(k_u)[x'(k_u - l/\Delta) - x'_{ref}(k_u)]^2}{c^2[\beta'_{ref}(k_u)C(k_u) + \beta'(k_u - l/\Delta)]}. \tag{14}$$

The linear in w component of the phase of (12) describes both the down-range and the Range Cell Migration (RCM) in down-range/Doppler domain. Under the approximation that $\beta'(k_u) \approx \beta'_{ref}(k_u)$ [21], the linear phase of the $(l = 0)$ component of (12) will be a function of the down-range only since the RCM of such a component is corrected. However, other $(l \neq 0)$ components will appear at shifted down-ranges and will still have residual RCM. At a given Doppler frequency, the RCM trajectory followed by the signal associated with the lth component is displaced from that of the $(l = 0)$ in down-range by:

$$\Delta x^l(k_u) = x_{ref}\beta'_\Delta(k_u; l)C(k_u) + \\ x\frac{\beta'(k_u - l/\Delta)C(k_u - l/\Delta) - \beta'_{ref}(k_u)C(k_u)}{\beta'_{ref}(k_u)C(k_u) + \beta'(k_u - l/\Delta)}. \tag{15}$$

As it will be demonstrated in Section IV-B, the residual RCM can cause the alias that corresponds to an $(l \neq 0)$ component to span multiple down-range resolution cells. The down-ranges spanned by any alias can be quantified by calculating (15) at different Doppler frequencies spanned by such a component.

In such a case, a loss of azimuth resolution will be encountered since part of the Doppler bandwidth will not be utilized when performing azimuth compression. The quadratic phase of the component $(l = 0)$ will be removed by the range compression phase multiply of (11). However, due to the mismatch between the quadratic range compression phase and the quadratic phase of $(l \neq 0)$ components, such components will still have residual quadratic phase that is responsible for a slight range defocus.

The final step in focusing the image is azimuth compression and residual phase removal which are, similar to the previous steps, performed based on the $(l = 0)$ component [21]:

$$S_c^l(x, k_u) = S_{rc}^l(x, k_u) e^{j[\sqrt{4k_c^2 - k_u^2} x - \Theta_\Delta(x, k_u; 0)]}, \qquad (16)$$

where the change of variables $x = ct/2$ is performed to emphasize the dependency of the azimuth compression filter and the residual phase removal on the down-range. The inverse Fourier transform of (16) in the Doppler domain produces the focused image which is defined as $s_c(x, u)$. In such an image, the $(l = 0)$ component will produce the fully focused scatterer at its true location. On the other hand, $(l \neq 0)$ components will generate replicas (ambiguities) that are shifted and defocused.

C. Staggered Coprime Sampling in Azimuth & Alias Removal

The PRF used is one of the factors that control the azimuth shift of different aliases. The lth alias is displaced in the azimuth direction by [14]:

$$\Delta u^l = \frac{\lambda_c l}{2\Delta_u} x. \qquad (17)$$

Using (15) and (17), the locations of the aliases in the focused image can be identified. Let the reference PRF, $PRF_0 = v_p/\Delta_{u0}$, be high enough to sample the Doppler bandwidth of the signal obtained from the scene of interest. Such a PRF could be chosen even higher to account for the non-ideal antenna beam-pattern. If PRF_0 is used, azimuth ambiguities, $(l \neq 0)$ of (17), will be out of the azimuth Field of View (FoV), hence, they can be disregarded. However, such a PRF will limit the maximum range swath width that can be unambiguously imaged. Therefore, in SCopSAR, the synthetic aperture is divided into staggered sub-apertures. As will be detailed later on, in each sub-aperture, one of two sub-Nyquist PRFs is used. The received signal which corresponds to the sub-apertures sampled using each of the PRFs is then used to produce a separate image that is free from range aliasing but contains azimuth aliases. Subsequently, the two images are processed jointly in a similar manner to CopSAR [14] to produce the alias-free image. SCopSAR can be applied in both spotlight and stripmap modes.

The sub-Nyquist PRFs used in SCopSAR are defined with respect to PRF_0 as $PRF_1 = PRF_0/N_1$ and $PRF_2 = PRF_0/N_2$ where N_1 and N_2 are coprime integers. Both PRF_1 and PRF_2 should be chosen low enough that (8) is fulfilled while the Radar is at any point along the synthetic aperture. This will ensure that the full range swath width is covered without introducing range ambiguities. In spotlight SAR, all the scatterers are observed for the whole duration of the aperture, therefore, the full synthetic aperture is divided into two halves, during the first half, pulses are transmitted at the rate of PRF_1 and the received signal is used to form the first image which is denoted as $s_{c1}(x, u)$. PRF_2 is then used during the second half to produce the second image $s_{c2}(x, u)$.

In stripmap SAR, a scatterer will be observed during a portion of the synthetic aperture that is given by its integration time, therefore, the full synthetic aperture is divided into sub-apertures each has a duration of $T_{int}/2$. PRF_1 is used during odd indexed sub-apertures $\{1^{st}, 3^{rd}, 5^{th}, \ldots\}$ and PRF_2 is used during even indexed sub-apertures $\{2^{nd}, 4^{th}, 6^{th}, \ldots\}$. The pulses received during odd indexed sub-apertures are used to produce the first sub-Nyquist image $s_{c1}(x, u)$, on the other hand, $s_{c2}(x, u)$ is produced using the pulses from the even indexed sub-apertures. In stripmap mode, during each sub-aperture, different scatterers in the illuminated scene will be weighted by different parts of the AAP. As a result, the same *scalloping effect* that is experienced in ScanSAR mode will affect the stripmap implementation of SCopSAR. Such an effect will introduce periodical modulation to the image amplitude, therefore, the amplitude of the scatterers at different azimuth locations will be weighted slightly differently [4]. Nonetheless, such an effect can be tolerated in SCopSAR since the focus of such a mode is on imaging brilliant bright scatterers in dark backgrounds, therefore, even if a scatterer is affected by such a *scalloping effect* it can still be observed in the image.

In both spotlight and stripmap modes, since the PRFs used are lower than the Doppler Nyquist rate, aliasing introduced by $(l \neq 0)$ components will cause ambiguities to appear in each image. The azimuth displacements of such ambiguities in $s_{c1}(x, u)$ and $s_{c2}(x, u)$ are, respectively, given as follows:

$$\Delta u_1^{l_1} = \frac{\lambda_c l_1}{2\Delta_{u1}} x, \quad \Delta u_2^{l_2} = \frac{\lambda_c l_2}{2\Delta_{u2}} x, \qquad (18)$$

where $l_1, l_2 \in \mathbb{Z}$, $\Delta_{u1} = N_1 \Delta_{u0}$, and $\Delta_{u2} = N_2 \Delta_{u0}$. Based on the coprime theory [23], the azimuth ambiguities of a given scatterer will not coincide at the same azimuth location in the two sub-Nyquist images except when $l_1 = N_1 l$ and $l_2 = N_2 l$. The locations where azimuth ambiguities coincide correspond to the locations that will be obtained if PRF_0 is used. Consequently, alias removal is performed as in CopSAR [14]. Each pixel in $s_{c1}(x, u)$ is compared to the corresponding pixel in $s_{c2}(x, u)$ and the value in the pixel that has the smaller magnitude is used to produce the alias-free image which is given as:

$$r(x, u) = \begin{cases} s_{c1}(x, u), & \text{if } |s_{c1}(x, u)| < |s_{c2}(x, u)| \\ s_{c2}(x, u), & \text{otherwise.} \end{cases} \qquad (19)$$

True targets will coincide at the same location in both images, therefore, choosing the pixel that has the smaller magnitude will still pick the target. Aliases, on the other hand, will be filtered out since they will not coincide in the two images and picking the pixel with the smaller magnitude will result in a pixel of the dark background. A false target will, however, appear if an alias of one scatterer collides with an alias of another scatterer as explained in [24].

The use of staggered PRFs in allows SCopSAR to extend the range swath width by a factor of $\min\{N_1, N_2\}$. On the other hand, in the basic implementation of CopSAR [14] which uses the same carrier frequency and the same waveform to transmit the pulses that correspond to both PRF_1 and PRF_2, the use of interlaced PRFs will result in the minimum time separation between the pulse transmission locations to be $1/PRF_0$, consequently, the maximum unambiguous range swath width in such a case is the same as when the Nyquist PRF is used as demonstrated in [15]. However, since only half the synthetic aperture is used to produce each image in SCopSAR, a loss of half the azimuth resolution will be incurred. CopSAR and OrthoCopSAR provide reduction in the amount of data to be stored and communicated as explained in [14], [15]. SCopSAR also provides a data reduction. Let N_{Total} denote the total number of pulses transmitted by a conventional SAR that operates at a Nyquist rate. The number of pulses transmitted if SCopSAR is used instead will be $N_{Total}(1/2N_1 + 1/2N_2)$, therefore, the number of received pulses that need to be stored and possibly communicated is reduced when using SCopSAR.

III. PRACTICAL CONSIDERATIONS

In this section, some practical considerations that need to be taken into account when implementing SCopSAR are introduced.

A. Transmitted Energy & Signal to Noise Ratio

SCopSAR transmits only a fraction of the number of pulses transmitted in the Nyquist case, consequently, the amount of energy used to illuminate different scatterers in the scene of interest will reduce. Therefore, a solution that is commonly used in the Radars that have the flexibility to change the PRF used is suggested here to compensate for the energy loss. If the same PRI is used to sample the whole synthetic aperture, the energy in a transmitted pulse will be given as follows [18]:

$$E_{tx} = P_{pk} \cdot T = P_{av} \cdot PRI, \qquad (20)$$

where P_{pk} is the peak transmitted RF power, P_{av} is the average power which is the equivalent power level if a Continuous Wave (CW) signal is used instead of the pulsed signal to transmit the same amount of energy during a PRI [18]. Moreover, T/PRI is the duty cycle. It is clear that a lower PRF will result in a lower average power.

SAR illuminates the scene of interest using a large number of pulses, therefore, one of the factors that control the amount of energy transmitted towards a scatterer is the PRF used. Accordingly, under the assumption that the use of the Nyquist PRF, PRF_0, along with a peak power of P'_{pk} and a pulse of duration T' will fulfill the minimum energy requirements, P_{av} should fulfill the following condition to ensure that, regardless of the sampling pattern, the energy used to illuminate different scatterers is, at least, equal to that of the Nyquist case:

$$P_{av} \geq P'_{pk} \cdot T' \cdot PRF_0. \qquad (21)$$

In SCopSAR, the average power should be calculated over the duration of two subsequent sub-apertures to account for the fact that only half the synthetic aperture is used to produce each sub-Nyquist image. Therefore, for SCopSAR and compared to the Nyquist case, either the peak power or the duration of the transmitted pulse should be increased by a factor of $2N_1$ and $2N_2$ when using PRF_1 and PRF_2, respectively. This will compensate for the reduction in the transmitted energy due to both sub-Nyquist sampling and using only half the synthetic aperture.

The limitation mentioned in this section can be better appreciated by looking at it from a slightly different perspective. SAR relies on both the range and azimuth compression gains to achieve the required Signal to Noise Ratio (SNR) [4]. Both the Nyquist and SCopSAR cases achieve the same range compression gain. However, SCopSAR uses only $1/2N_1$ and $1/2N_2$ of the number of pulses used in the Nyquist case to produce the sub-Nyquist images $s_{c1}(x, u)$ and $s_{c2}(x, u)$, respectively. Therefore, compared to the Nyquist case, the azimuth compression gain in $s_{c1}(x, u)$ and $s_{c2}(x, u)$ is reduced by $1/2N_1$ and $1/2N_2$, respectively. Accordingly, the use of $2N_1$ and $2N_2$ times higher RF peak power or larger duty cycle when operating at PRF_1 and PRF_2, respectively, will allow SCopSAR to achieve the same SNR achieved by the corresponding SAR that operates at the Nyquist case (see Section 1.10 of [4] for more detail on the SNR issue in SAR). It is worth mentioning that peak power and duty cycle limitations of the hardware used should be adhered to which poses a limitation on the largest sub-sampling factor that can be used. This poses a limitation on the maximum swath width that can be covered and the maximum data reduction that can be achieved. The analysis in this section does not cover the problem of Target to Background Ratio (TBR) degradation due to clutter folding which is introduced due to the use of sub-Nyquist PRFs. TBR will be addressed in more details in Section IV-C.

B. Limits on Target Size & Sparsity

As will be demonstrated in Section IV-B, in the airborne SAR case and when the scene of interest is at a small distance from the platform, the azimuth aliases will be highly defocused and will occupy a larger area in the image compared to the corresponding true target, however, this is an exceptional case. If the scene of interest is at a large distance from the platform, the size of the aliases will be comparable to the true target. Therefore, the focus of this section is on providing a limit on the maximum target size that can be unambiguously imaged in the satellite SAR case when the azimuth aliases are only slightly defocused, *i.e.*, when the size of each of the aliases is comparable to the size of the true target which is, for instance, the case of the ERS-2 satellite example shown in Section IV-C. The location of the azimuth aliases in SCopSAR, which is given by (18), is the same as that of CopSAR [14], dual-frequency CopSAR [14], and OrthoCopSAR [15]. Accordingly, the minimum azimuth distance between the aliases of a given scatterer will be [14]:

$$\Delta_{min} = \min_{l_1, l_2} |\Delta u_1^{l_1} - \Delta u_2^{l_2}| = \frac{\lambda_c x}{2\Delta_{u0} N_1 N_2}. \qquad (22)$$

If the azimuth width of a target exceeds (22), some of the aliases that correspond to such a target will overlap. Consequently, the simple combination rule of (19) will not remove all aliases and this will result in the appearance of false targets. Therefore, although the use of larger sub-sampling factors will allow for more data reduction and wider range swath coverage, however, it will also reduce the maximum azimuth width of the target that can be unambiguously imaged.

Coprime sampling will ensure that the aliases that correspond to a given scatterer will not overlap in the two sub-Nyquist images, however, the aliases that correspond to different scatterers can still overlap. Therefore, a problem will arise if the scene of interest contains a large number of scatterers, $i.e.$, if the scene is less sparse. Assume that PRF_0 is chosen just high enough to fulfill the azimuth Nyquist sampling requirements. A single scatterer will appear in the sub-Nyquist images produced using PRF_1 and PRF_2 at N_1 and N_2 different locations, respectively. Therefore, the use of larger sub-sampling factors will increase the number of aliases per scatterer which, consequently, increases the likelihood of having aliases that correspond to different scatterers overlapping at the same location. In such a case, (19) will not remove such overlapping aliases which will allow for false targets to appear in the final SCopSAR image. The likelihood of having overlapping scatterers increases with the increase in the number of scatterers in the observed scene or with the use of larger sub-sampling factors. This poses another limitation on the largest sub-sampling factors that can be used for a given sparsity level.

One of the possible solutions to the target size and sparsity limitations is the use of the coherency map used in [15]. The coherency map relies on the fact that the aliases that correspond to different scatterers are highly uncorrelated, hence, the correlation map can be utilized to suppress aliases and preserve true targets. Another possible solution is the use of an additional along-track receive phase center to induce a differential phase that can be utilized to distinguish true scatterers from aliases as in MC-CopSAR [24]. Such limitations are only highlighted here, however, they will be addressed for the case of SCopSAR in detail in a future research.

IV. EXPERIMENTAL RESULTS

In this section, the proposed SCopSAR is demonstrated for the case of airborne spotlight SAR based on simulations. Furthermore, real ERS-2 raw data of a scene that contains ships in a dark sea background are used to demonstrate the case of a satellite operating in stripmap mode.

A. Simulation Results

Consider the case of spotlight imaging a broadside target area centered at $(X_c, 0)$ based on the airborne SAR parameters given in Table I. In all simulations, a single scatterer located at $(9000, 0)$ is considered. In the images shown, such a scatterer is centered at $(0, 0)$. Fig. 1 shows the case of sampling using the Nyquist PRF and a demonstration of the proposed SCopSAR. The focus is on two sections of the image, the first one is zoomed around the true scatterer and

TABLE I
SPOTLIGHT SCOPSAR SIMULATION PARAMETERS

| Parameter	Symbol	Value
Carrier Frequency	f_c	$10\ GHz$
Platform Velocity	v_p	$100\ m/s$
Chirp Bandwidth	BW_p	$50\ MHz$
Sampling Rate		$75\ MHz$
Chirp Duration	T	$0.3\ \mu s$
Aperture Length	$2L$	$320\ m$
Antenna Azimuth Width	D_u	$3\lambda_c\ m$
Minimum Down-Range	x_{min}	$8.3\ km$
Platform Altitude	Z_c	$5\ km$
Reference Down-Range	x_{ref}	$9\ km$
Instantaneous Doppler Bandwidth	BW_D^{inst}	$4447.5\ Hz$
Reference PRF	PRF_0	$4500\ Hz$
Sub-sampling Factors	$\{N_1, N_2\}$	$\{5, 7\}$
Sub-Nyquist PRFs	$\{PRF_1, PRF_2\}$	$\{900, 642.8571\}\ Hz$

the other is zoomed around the down-range of the first alias associated with sampling at PRF_0. Each image in Fig. 1 is normalized to the magnitude of the true scatterer at $(0, 0)$ which, since there is only one scatterer in the considered scene, corresponds to the maximum magnitude in each image. As demonstrated by Fig. 1(a), the use of PRF_0 will ensure that the Doppler bandwidth is sampled at higher than Nyquist rate, therefore, the resulting image is free from azimuth ambiguities. However, such a high PRF will introduce range ambiguities that are displaced in the down-range by multiples of $c/2PRF_0 = 33310.27\ m$. The first of such ambiguities is shown in the bottom of Fig. 1(a). Such an ambiguity is attenuated and defocused due to the mismatch between its parameters and those used to focus the image. Therefore, the use of Nyquist PRF will limit the maximum down-range which, consequently, limits the maximum unambiguous range swath width that can be covered. The image in Fig. 1(b) is obtained using the first half of the synthetic aperture which is sampled using PRF_1 and extends from $(0, -160)$ to $(0, 0)$. The image in Fig. 1(c) is obtained using the second half which is sampled using PRF_2 and extends from $(0, 0)$ to $(0, 160)$. The range ambiguities in the images obtained using each of PRF_1 and PRF_2 are displaced by multiples of $cN_1/2PRF_0$ and $cN_2/2PRF_0$, respectively. This allows a covering of $\min\{N_1, N_2\} = 5$ times wider range swath, however, for the individual reconstructions, the use of sub-Nyquist PRFs introduces azimuth aliasing. Due to the choice of the coprime sub-sampling factors, the aliases in each image are displaced to distinct azimuth locations as given by (18). Accordingly, by processing the two sub-Nyquist images as explained in Section II-C, the alias-free SCopSAR image shown in Fig. 1(d) is obtained. It is worth mentioning that the presence of a large number of scatterers would introduce false detection due to the overlap between aliases of different scatterers. A possible solution to this problem is the use of an additional along-track receive phase center as proposed in MC-CopSAR [24] but we do not consider this further here.
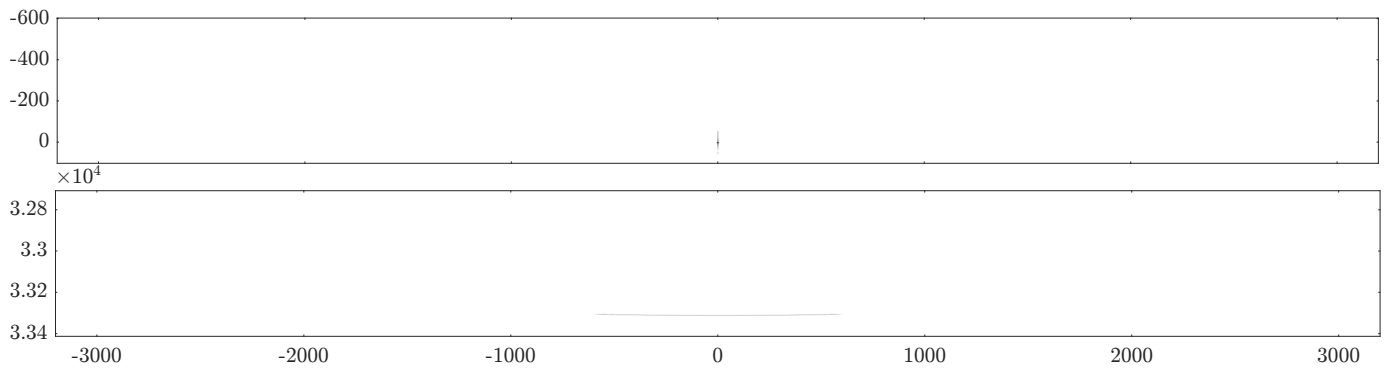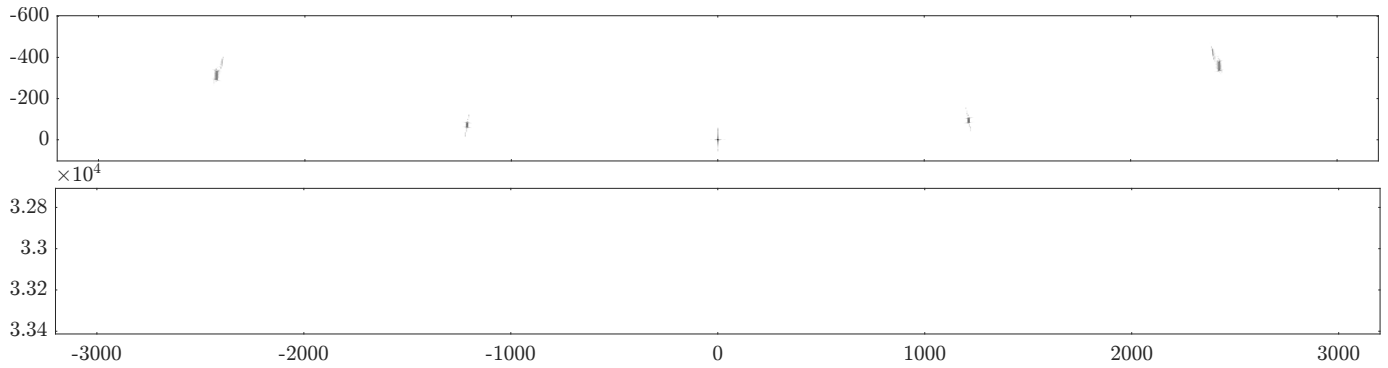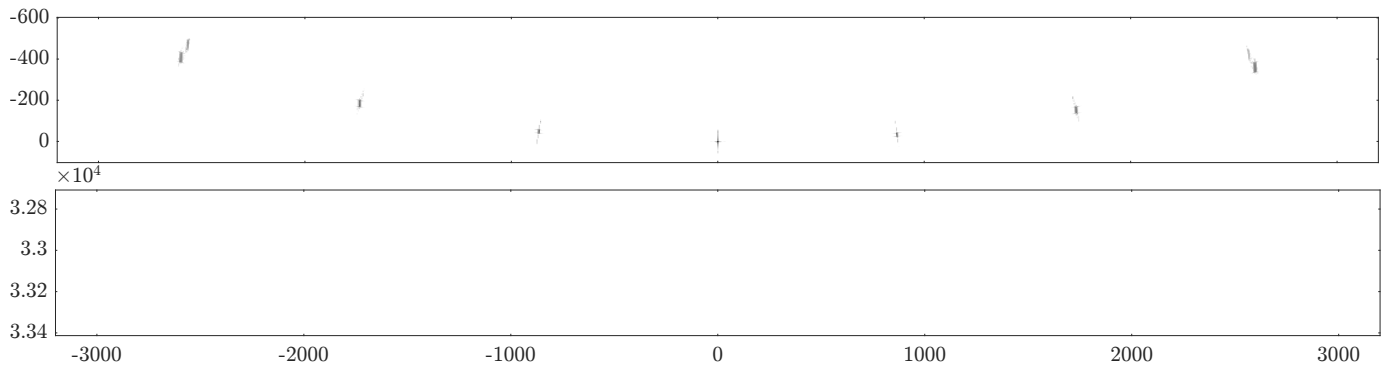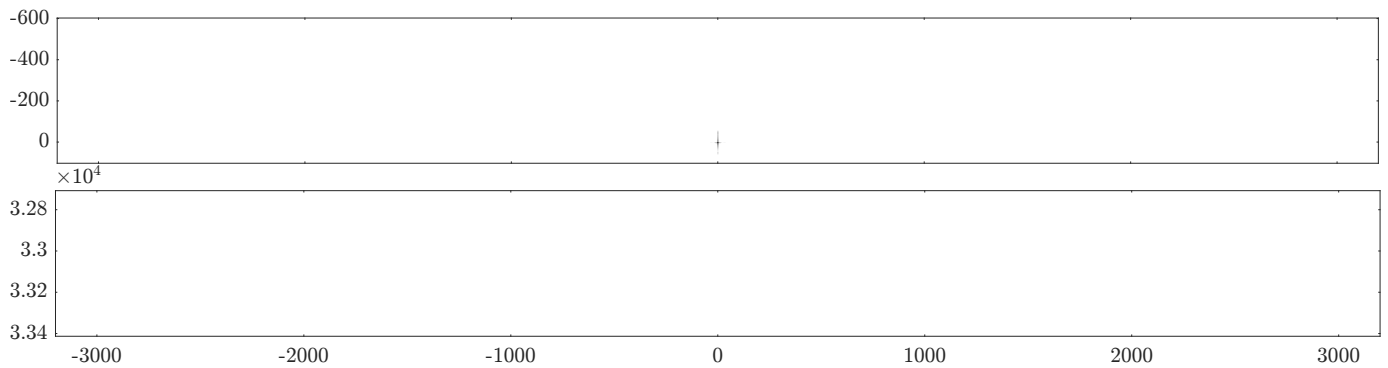
Fig. 1. (a) The image obtained using PRF_0 which is higher than the Doppler Nyquist rate. Such a high PRF ensures that no azimuth ambiguities will exist in the image, however, it introduces range ambiguities that limit the maximum range swath width that can be covered. The first down-range ambiguity is displaced by $c/2PRF_0 = 33310.27\ m$. (b) The image $s_{c1}(x, u)$ obtained using the first half of the synthetic aperture sampled at PRF_1. (c) The image $s_{c2}(x, u)$ obtained using the second half of the synthetic aperture sampled at PRF_2. (d) The alias-free SCopSAR image $r(x, u)$. The horizontal and vertical axes are, respectively, the azimuth and down-range domains. In all images, near down-range is shown in the top and far down-range is in the bottom.
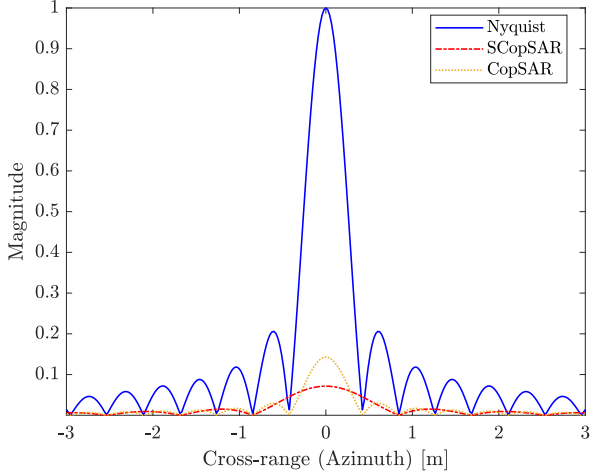
Fig. 2. Azimuth cut at the down-range of the true scatterer ($l = 0$) after image reconstruction and alias removal normalized to the maximum magnitude in the Nyquist case. Since the full synthetic aperture is utilized in both the Nyquist and CopSAR [14] cases, the azimuth resolution in such cases is twice that of SCopSAR.
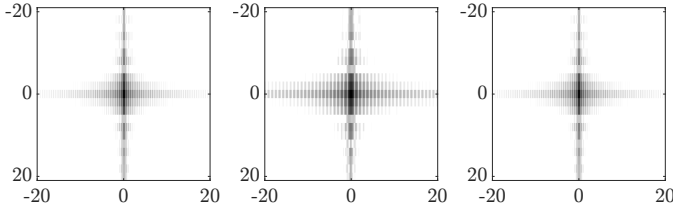

Fig. 3. The point spread function of the ($l = 0$) component in Nyquist (left), SCopSAR (middle), and CopSAR (right). In all cases, the true target is well preserved while, in SCopSAR, the azimuth resolution has been reduced by a factor of two. The horizontal and vertical axes are, respectively, the azimuth and down-range domains.

Fig. 2 shows an azimuth cut at the down-range that corresponds to the true target location in Nyquist, CopSAR, and SCopSAR cases after image reconstruction and alias removal. SCopSAR uses only half the synthetic aperture to produce each sub-Nyquist image, consequently, the azimuth resolution in SCopSAR is half that of Nyquist and CopSAR cases which use the full aperture. Moreover, due to the sub-Nyquist sampling and according to (19), in CopSAR, only $1/\max\{N_1, N_2\}$ of the number of pulses used in Nyquist case are used to produce CopSAR image. In SCopSAR, half the synthetic aperture is used to produce each sub-Nyquist image, therefore, only $1/\max\{2N_1, 2N_2\}$ of the number of pulses used in Nyquist case are used to produce SCopSAR image. The impact of using a smaller number of pulses is clear in Fig. 2. In this figure, the magnitudes are normalized to the maximum magnitude in the Nyquist case to emphasize the signal loss due to sub-sampling in CopSAR and sub-sampling and using half the synthetic aperture in SCopSAR. Fig. 3 shows the two-dimensional Point Spread Function (PSF) of the target after image reconstruction and alias removal. In both CopSAR and SCopSAR cases, the true target is well preserved while, in SCopSAR, azimuth resolution has been reduced by a factor of two.
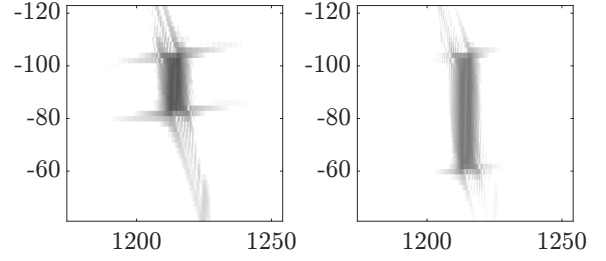

Fig. 4. The response of the alias that corresponds to ($l = 1$) component in SCopSAR (left) and CopSAR (right) when the sub-Nyquist PRF_1 is used. The spread in down-range is mainly due to the RCMC which is matched to the ($l = 0$) but not other ($l \neq 0$) components. The horizontal and vertical axes are, respectively, the azimuth and down-range domains.

B. Range Defocus of Azimuth Ambiguities

Fig. 4 shows the alias that corresponds to the ($l = 1$) component in the sub-Nyquist images produced using PRF_1 in SCopSAR and CopSAR. As expected from the analysis of Section II-B, aliases are defocused in both the down-range and the azimuth domains. The down-range extent of an alias is related to the shift introduced by the RCMC to the corresponding ($l \neq 0$) component. Such a shift is a function of Doppler and it can be quantified using (15). The instantaneous spatial Doppler frequency generated due to a scatterer at (x, y) while the Radar is at azimuth location u is given as [3]:

$$k_u^{inst}(u; x, y) = \frac{4\pi}{\lambda_c} \frac{y - u}{\sqrt{x^2 + (y - u)^2}}. \qquad (23)$$

This gives the instantaneous frequency that corresponds to the ($l = 0$) component, however, due to azimuth sampling and according to (9), the frequencies $k_u^{inst}(u; x, y) + 2\pi l/\Delta_u$ will also be generated. Therefore, the instantaneous Doppler of any component can be identified. The left of Fig. 4 shows a zoomed version of the ($l = 1$) alias in the SCopSAR sub-Nyquist image $s_{c1}(x, u)$ which is produced using the first half of the synthetic aperture sampled at PRF_1. At the start of the synthetic aperture, the instantaneous frequency associated with such an alias is $k_u^{inst}(-160; 9000, 0) + 2\pi/\Delta_{u1} = 63.9994 \ rad/s$. Based on (15), the ($l = 1$) component is shifted at such a frequency by $\Delta x^1(63.9994) = -104.1141 \ m$. At the end of the first sub-aperture, $k_u^{inst}(0; 9000, 0) + 2\pi/\Delta_{u1} = 56.5487 \ rad/s$ and $\Delta x^1(56.5487) = -82.2744 \ m$. This quantifies the down-range spread of such an alias with a reasonable accuracy. A zoomed version of the ($l = 1$) alias in the case of using PRF_1 in CopSAR is shown on the right of Fig. 4. Unlike in SCopSAR, the synthetic aperture used to produce such an image extends until $L = 160$ at which $k_u^{inst}(160; 9000, 0) + 2\pi/\Delta_{u1} = 49.098 \ rad/s$. Consequently, the range spread in this case extends until $\Delta x^1(49.098) = -60.5399 \ m$. In both cases, the center of such an alias is displaced in azimuth by $\Delta u_1^1 = 1214.16 \ m$.

C. Experiments Using Real ERS-2 Raw Data

The ERS-2 satellite raw data of a scene that contains ships in a dark sea background near Long Beach Harbor,

TABLE II
SCNRs OF SCopSAR COMPARED TO NYQUIST

Case	Sub-sampling Factors	SCNR [dB]
Nyquist		34.46
SCopSAR	$\{3, 4\}$	27.58
	$\{5, 6\}$	25.16
	$\{7, 8\}$	23.9

Los Angeles, USA is used to demonstrate imaging from sub-Nyquist samples in real satellite data. Such data were collected on the 10th of October 2009 and are available online in [25]. Since the PRF used during ERS-2 data acquisition fulfills the azimuth Nyquist sampling criterion [4], such a PRF is used to define the reference PRF, hence, $PRF_0 = 1679.9 \ Hz$. The sub-sampling factors used to produce the sub-Nyquist images are $\{N_1, N_2\} = \{3, 4\}$. The pulses received during odd indexed sub-apertures are used to produce the first sub-Nyquist image $s_{c1}(x, u)$ which is shown in Fig. 5(a), on the other hand, Fig. 5(b) shows $s_{c2}(x, u)$ which is produced using the pulses from the even indexed sub-apertures. As compared to Fig. 5(c) which shows the conventional SAR image obtained by sampling the full synthetic aperture using PRF_0, both sub-Nyquist images contain different ships at their true locations in addition to azimuth replicas due to the use of the sub-Nyquist PRFs. The final alias-free SCopSAR image is shown in Fig. 5(d) and it can be seen that aliases are highly suppressed and true targets are mostly preserved. In the Nyquist case, a background clutter pixel will have contribution from a single azimuth location. On the other hand, due to the aliasing introduced by the sub-Nyquist sampling, each pixel of the background clutter in the sub-Nyquist images has contribution from multiple spatially separated azimuth locations and this leads to a higher clutter level. Consequently, this will result in a reduction in the TBR as explained in [14]. The impact of this is clear from the SCopSAR image of Fig. 5(d) since the contrast between the ships (targets) and the background is reduced compared to the Nyquist case of Fig. 5(c).

To better illustrate the degradation in the TBR, Fig. 6(a) and Fig. 6(b), respectively, show zoomed versions of the two ships near the top right corner of the Nyquist and SCopSAR images shown in Fig. 5. Furthermore, Fig. 6(c) and Fig. 6(d) show the SCopSAR images of the same ships obtained using the sub-sampling factors $\{5, 6\}$ and $\{7, 8\}$, respectively. It can be clearly seen that the TBR of the SCopSAR images is worst than the Nyquist image. Moreover, the TBR of the SCopSAR images gets worse with the increase in the sub-sampling factors used. The Signal to Clutter and Noise Ratio (SCNR) is used to quantify the degradation in the TBR in different examples. The SCNR is the ratio between the target's signal power and the power of the clutter and noise signal and it is estimated here using the portion of the image shown in Fig. 6. Table II lists the SCNR for a range of examples. It is clear that the use of larger sub-sampling factors will degrade the SCNR further.
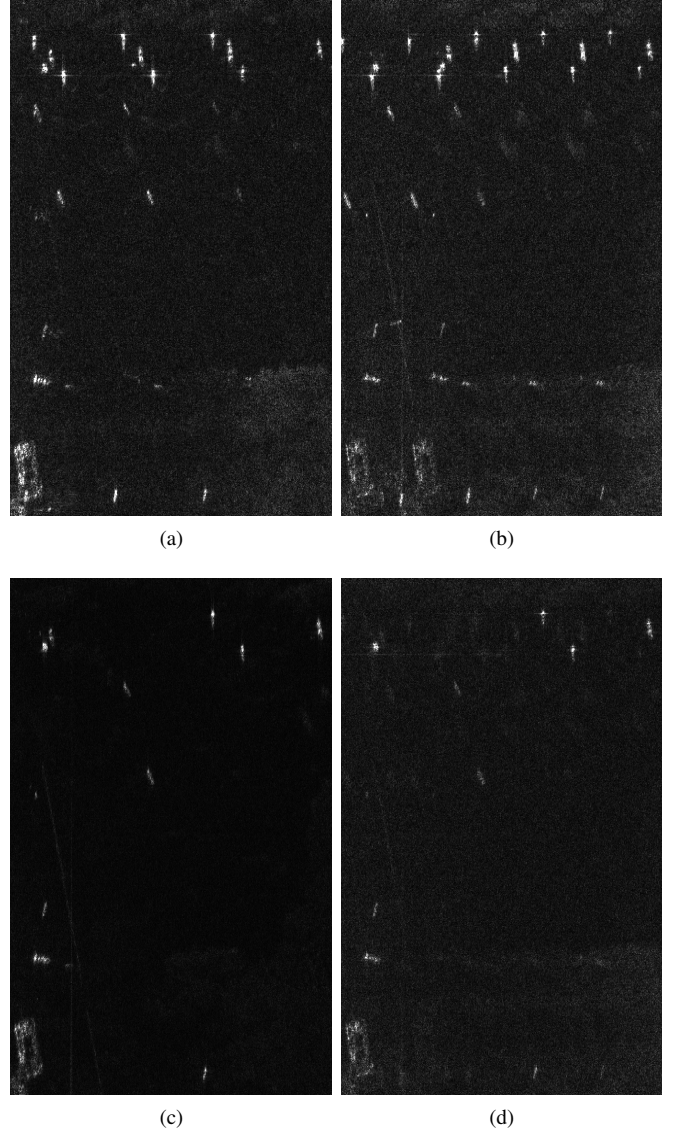

(a)   (b)

(c)   (d)

Fig. 5. Demonstration of SCopSAR in stripmap SAR mode using real ERS-2 raw data. $s_{c1}(x, u)$ (a) and $s_{c2}(x, u)$ (b). Conventional SAR image produced without sub-sampling (c) and the alias-free SCopSAR image $r(x, u)$ (d). The horizontal and vertical axes are, respectively, the azimuth and range domains.

V. CONCLUSION

SCopSAR allows one to extend the maximum range swath width that can be imaged without the need for the use of multiple carrier frequencies, waveforms, channels, or multi-beams techniques. This leads to simple system requirements. SCopSAR further allows for a reduction in the amount of data that need to be stored and communicated. SCopSAR is suitable for scenes that contain a limited number of bright scatterers over a dark background. In this paper, the exact location of azimuth aliases and the extent of their range defocus are quantified and demonstrated using simulations. Furthermore, SCopSAR is demonstrated for the case of airborne spotlight SAR using simulations and for the case of stripmap SAR using real ERS-2 satellite raw data. Compared to a SAR operating at a Nyquist rate, the price paid to allow for such a wide-swath capability is half the azimuth resolution and a

reduction in the TBR. In SCopSAR, the use of larger sub-sampling factors is desirable since it allows for more data reduction and wider range swath coverage, however, it also requires transmitting pulses at a higher RF peak power or using a larger duty cycle to compensate for the SNR loss due to sub-Nyquist sampling and using only half the synthetic aperture. Moreover, the use of larger sub-sampling factors will place a more strict limit on the maximum azimuth width of the imaged targets and the maximum number of scatterers that can be unambiguously imaged, *i.e.,* it will require the scene to be more sparse. Furthermore, the use of larger sub-sampling factors will introduce more degradation to the SCNR and this is demonstrated using real ERS-2 satellite SAR data. Although SCopSAR is clutter-limited, however, it fills an important gap, for instance, it is attractive in a multi-mode setting where there is a need to cover large areas that contain bright scatterers in a dark background during a short visit time. Moreover, one of the desirable applications of SCopSAR is for the case of imaging at a large incidence angle since, in such a scenario, the antenna beam-pattern is not as useful in rejecting the scatterers at the far range which may introduce range ambiguities. An interesting future research direction would be in exploring the use of the proposed SCopSAR sampling strategy to allow for range swath extension in SAR based Ground Moving Target Indication (GMTI) in a similar manner to the recently proposed CopGMTI [26]. Moreover, SCopSAR uses only half the synthetic aperture to produce each sub-Nyquist image which results in a loss of half the azimuth resolution. Therefore, it is of interest to investigate the possibility of coherently processing the two sub-Nyquist images to preserve azimuth resolution.
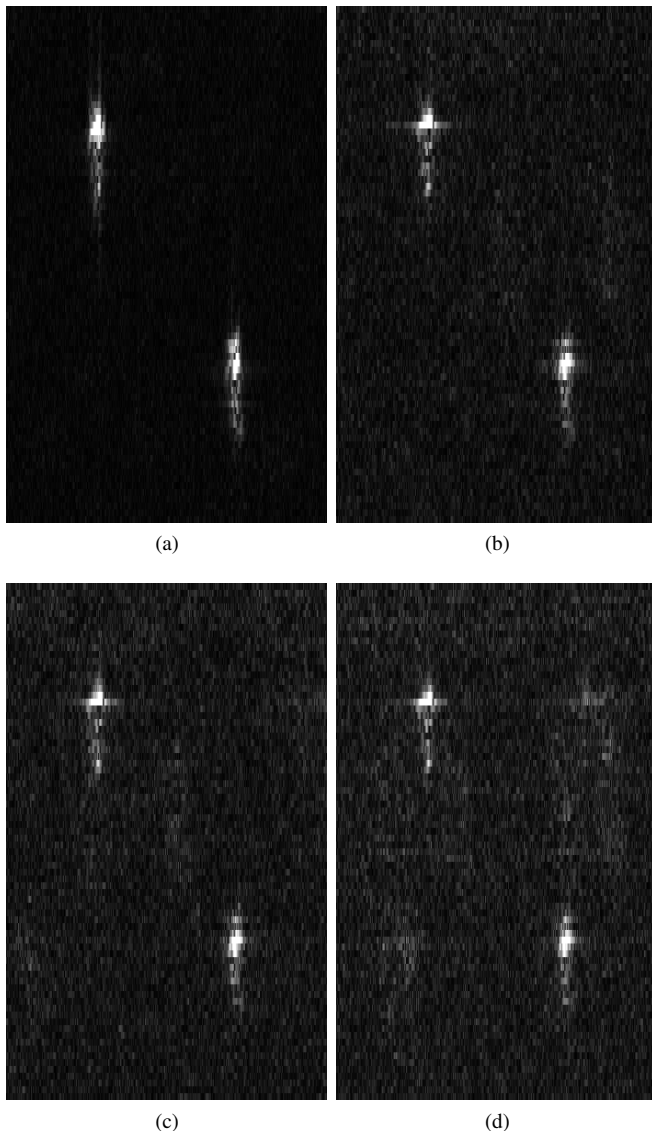

Fig. 6. (a) and (b), respectively, show zoomed versions of the two ships near the top right corner of the Nyquist case shown in Fig. 5(c) and the SCopSAR case with $\{N_1, N_2\} = \{3, 4\}$ which is shown in Fig. 5(d). (c) and (d) show the SCopSAR images of the same ships when the sub-sampling factors used are $\{5, 6\}$ and $\{7, 8\}$, respectively. Compared to the Nyquist case, the TBR in SCopSAR is lower and this is clearly demonstrated by this example. Moreover, the TBR degrades with the increase in the sub-sampling factors used. Table II lists the estimates of the SCNR of the different examples shown in this figure. It is worth mentioning that, in (d) which uses $\{7, 8\}$, some highly attenuated residual ambiguities can be observed in the SCopSAR image. This is the issue discussed in Section III-B and it is introduced due to the fact that the used sub-sampling factors are large and the considered scene is not very sparse around the ranges that correspond to the ships. The horizontal and vertical axes are, respectively, the azimuth and range domains.

REFERENCES

[1] A. Moreira, P. Prats-Iraola, M. Younis, G. Krieger, I. Hajnsek, and K. P. Papathanassiou, "A tutorial on synthetic aperture radar," *IEEE Geosci. Remote Sens. Mag.*, vol. 1, no. 1, pp. 6–43, Mar. 2013.

[2] I. G. Cumming and F. H. Wong, *Digital processing of synthetic aperture radar data : algorithms and implementation*. Norwood, MA , USA: Artech House, 2005.

[3] M. Soumekh, *Synthetic aperture radar signal processing with MATLAB algorithms*. New York, NY, USA: Wiley, 1999.

[4] G. Franceschetti and R. Lanari, *Synthetic Aperture Radar Processing*, ser. Electronic Engineering Systems. Taylor & Francis, 1999.

[5] W. G. Carrara, R. S. Goodman, and R. M. Majewski, *Spotlight synthetic aperture radar: signal processing algorithms*. Boston, MA, USA: Artech House, 1995.

[6] R. K. Moore, J. P. Claassen, and Y. h. Lin, "Scanning spaceborne synthetic aperture radar with integrated radiometer," *IEEE Trans. Aerosp. Electron. Syst.*, vol. AES-17, no. 3, pp. 410–421, May 1981.

[7] F. De Zan and A. Monti Guarnieri, "Topsar: Terrain observation by progressive scans," *IEEE Trans. Geosci. Remote Sens.*, vol. 44, no. 9, pp. 2352–2360, 2006.

[8] G. Krieger, N. Gebert, M. Younis, F. Bordoni, A. Patyuchenko, and A. Moreira, "Advanced concepts for ultra-wide-swath sar imaging," in *Proc. European Conf. Synthetic Aperture Radar*, Friedrichshafen, Germany, June 2008, pp. 1–4.

[9] A. Currie and M. A. Brown, "Wide-swath sar," *IEE Proc. F Radar and Signal Process.*, vol. 139, no. 2, pp. 122–135, 1992.

[10] G. Krieger, N. Gebert, and A. Moreira, "Multidimensional waveform encoding: A new digital beamforming technique for synthetic aperture radar remote sensing," *IEEE Trans. Geosci. Remote Sens.*, vol. 46, no. 1, pp. 31–46, Jan. 2008.

[11] N. Gebert, G. Krieger, and A. Moreira, "Digital beamforming on receive: Techniques and optimization strategies for high-resolution wide-swath sar imaging," *IEEE Trans. Aerosp. Electron. Syst.*, vol. 45, no. 2, pp. 564–592, Apr. 2009.

[12] D. Cerutti-Maori, I. Sikaneta, J. Klare, and C. H. Gierull, "Mimo sar processing for multichannel high-resolution wide-swath radars," *IEEE Trans. Geosci. Remote Sens.*, vol. 52, no. 8, pp. 5034–5055, Aug. 2014.

[13] J. Brown, "Multi-channel sampling of low-pass signals," *IEEE Trans. Circuits Syst.*, vol. 28, no. 2, pp. 101–106, Feb. 1981.

[14] G. D. Martino and A. Iodice, "Coprime synthetic aperture radar (Cop-SAR): A new acquisition mode for maritime surveillance," *IEEE Trans. Geosci. Remote Sens.*, vol. 53, no. 6, pp. 3110–3123, Jun. 2015.

[15] ——, "Orthogonal coprime synthetic aperture radar," *IEEE Trans. Geosci. Remote Sens.*, vol. 55, no. 1, pp. 432–440, Jan. 2017.

[16] J. Mittermayer and J. M. Martinez, "Analysis of range ambiguity suppression in sar by up and down chirp modulation for point and distributed targets," in *Proc. IEEE Geosci. Remote Sens. Symp.*, vol. 6, Jun. 2003, pp. 4077–4079.

[17] G. Krieger, "Mimo-sar: Opportunities and pitfalls," *IEEE Trans. Geosci. Remote Sens.*, vol. 52, no. 5, pp. 2628–2645, 2014.

[18] C. Alabaster, *Pulse Doppler radar : principles, technology, applications*. Edison, NJ, USA: SciTech, 2012.

[19] G. V. M. Linda L. Harkness, *Airborne Pulsed Doppler Radar, Second Edition*. Boston, MA, USA: Artech House, 1996.

[20] R. K. Raney, "A new and fundamental fourier transform pair," in *Proc. IGARSS*, vol. 1, Clear Lake, TX, USA, May 1992, pp. 106–107.

[21] R. K. Raney, H. Runge, R. Bamler, I. G. Cumming, and F. H. Wong, "Precision sar processing using chirp scaling," *IEEE Trans. Geosci. Remote Sens.*, vol. 32, no. 4, pp. 786–799, 1994.

[22] B. Mulgrew, P. Grant, and J. Thompson, *Digital signal processing: concepts and applications*. Basingstoke, UK: Macmillan, 2003.

[23] T. Nagell, *Introduction to Number Theory*, ser. AMS Chelsea Publishing Series. AMS Chelsea, 2001.

[24] A. Aldharrab and M. E. Davies, "Multichannel coprime synthetic aperture radar (MC-COPSAR)," in *Proc. IEEE Radar Conf.*, Boston, MA, USA, Apr. 2019, pp. 1–6.

[25] [Online]. Available: http://eo-virtual-archive4.esa.int/

[26] A. Aldharrab and M. E. Davies, "Multichannel coprime SAR/GMTI (CopGMTI)," in *Proc. IEEE Intl. Radar Conf.*, Washington, DC, USA, Apr. 2020, pp. 827–832.

Mike E. Davies (F'15) holds the Jeffrey Collins Chair in Signal and Image Processing at UoE, where he also leads the Edinburgh Compressed Sensing Research Group, and was Head of the Institute for Digital Communications (IDCOM) 2013-2016. He received an M.A. in engineering from Cambridge University in 1989 where he was awarded a Foundation Scholarship (1987), and a Ph.D. degree in nonlinear dynamics from University College London (UCL) in 1993. He was awarded a Royal Society University Research Fellowship in 1993 and was a Texas Instruments Distinguished Visiting Professor at Rice University in 2012. He leads the UK University Defence Research Collaboration (UDRC) programme on signal processing for defence in collaboration with the U.K. Defence Science and Technology Laboratory (DSTL). He is a recipient of a European Research Council (ERC) advanced grant on Computational Sensing, and a Royal Society Wolfson Research Merit award. He has been elected a EURASIP Fellow, a Fellow of the Royal Society of Edinburgh and a Fellow of the Royal Academy of Engineering.

His research has focused on nonlinear time series, source separation, compressed sensing and computational imaging. He has also explored the application of these ideas to advanced medical imaging, RF sensing applications and machine learning.

Abdulmalik Aldharrab (Member, IEEE) received the B.Eng. degree (Hons.) in electrical engineering-communication and electronics from King Saud University (KSU), Riyadh, Saudi Arabia, in 2011, and the M.Sc. degree (Distinction) in signal processing and communications and the Ph.D. degree in engineering (digital communications) from The University of Edinburgh (UoE), Edinburgh, U.K., in 2016 and 2021, respectively.

After obtaining the bachelor's degree in 2011, he joined King Abdulaziz City for Science and Technology (KACST), Riyadh, Saudi Arabia, where, from 2011 to 2015, he was working on the development of next-generation airborne radar systems in collaboration with Selex ES, Edinburgh, U.K., which is currently known as Leonardo UK Ltd. He is a Researcher at KACST. His research interests include sub-Nyquist signal processing techniques and their applications in synthetic aperture radar (SAR) imaging, ground moving target indication (GMTI), and radar signal processing.

Dr. Aldharrab was the recipient of the UoE 2015–2016 Class Medal of the M.Sc. degree in signal processing and communications. He was awarded fully funded KACST M.Sc. and UoE Ph.D. scholarships in 2015 and 2017, respectively. His article "Multichannel Coprime SAR/GMTI (CopGMTI)" was nominated for the Best Student Paper Award Competition in the 2020 IEEE International Radar Conference.